



# Palladium supported on metal–organic framework as a catalyst for the hydrogenation of nitroarenes under mild conditions

Lingxiang Bao<sup>1</sup> | Zongbao Yu<sup>1</sup> | Teng Fei<sup>1</sup> | Zhiyuan Yan<sup>1</sup> | Jiazhe Li<sup>1</sup> | Chenghui Sun<sup>1,2</sup> | Siping Pang<sup>1,2</sup>

<sup>1</sup>School of Materials Science and Engineering, Beijing Institute of Technology, Beijing, 100081, China

<sup>2</sup>Key Laboratory for Ministry of Education of High Energy Density Materials, Beijing Institute of Technology, Beijing, 100081, China

## Correspondence

Chenghui Sun and Siping Pang, School of Materials Science and Engineering, Beijing Institute of Technology, Beijing 100081, China.

Email: sunch@bit.edu.cn; pangsp@bit.edu.cn

## Funding information

National Natural Science Foundation of China, Grant/Award Numbers: 21576026, 21975023

Sustainable development demands an environmentally friendly and efficient method for the hydrogenation of organic molecules, including the hydrogenation of functionalized nitroarenes. In this study, a highly active and selective metal–organic framework-supported palladium catalyst was prepared for the catalytic hydrogenation of nitroarenes. High selectivity (>99%) and excellent yield (98%) of aniline were realized after 2 hours in ethanol under hydrogen (1 atm) at room temperature. The reductions were successfully carried out in the presence of a wide range of other reducible functional groups. More importantly, the catalyst was very stable without the loss of its catalytic activity after five cycles.

## KEY WORDS

heterogeneous catalysts, MOFs, nitroarenes, palladium, reduction

## 1 | INTRODUCTION

Functionalized anilines are versatile intermediates for agrochemicals, pharmaceuticals, pigments, dyes and fine chemicals.<sup>[1]</sup> Because of their importance, many methods for the reduction of nitroarenes have been developed.<sup>[2]</sup> In general, the methods can be categorized into two types.<sup>[3]</sup> One is a stoichiometric reduction of the corresponding nitroarenes using sodium hydrosulfite, iron, tin or zinc.<sup>[4]</sup> However, this method often causes environmental issues such as large amounts of waste acids and residues generated during the reaction. The second is catalytic hydrogenation of nitro compounds over supported metal catalysts, e.g. Au,<sup>[5]</sup> Ni,<sup>[6]</sup> Fe,<sup>[7]</sup> Ru<sup>[8]</sup> and Co<sup>[9]</sup> catalysts. Nevertheless, the reported catalysts usually require harsh conditions, such as a high reaction temperature<sup>[10]</sup> and a high hydrogen pressure.<sup>[11]</sup> Therefore, it is highly desirable to develop an

environmentally friendly and efficient method for the production of functionalized anilines.

In recent years, metal–organic frameworks (MOFs) have emerged as the most promising stabilizing agents for supported metal nanoparticles owing to their well-defined structure, large surface areas and chemical tunability.<sup>[12]</sup> Their special structures limit the interaction/contact between incorporated metal nanoparticles, avoiding the agglomeration and leaching of the metal nanoparticles.<sup>[13]</sup> Among their advantages, the most significant one is the designability of the organic ligands in the MOF material, thus controlling the size and properties of the MOFs, which is unmatched by traditional porous materials.<sup>[14]</sup> For example, the MOF  $[Zn(pip)(bpy)]_n$  (MOF-1, H<sub>2</sub>pip = 5-(prop-2-yn-1-yloxy)isophthalic acid, bpy = 4,4'-bipyridine) is constructed by an alkyne-functionalized ligand and Zn ions which shows a high noble metal loading.<sup>[15]</sup>

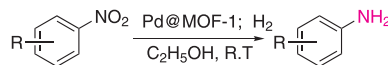
MOF-supported metal nanoparticles have been found to show excellent catalytic performance towards a wide range of organic reactions, including oxidation,<sup>[16]</sup> photocatalytic oxidation and reduction,<sup>[17]</sup> hydrogenation<sup>[18]</sup> and so on. However, there remains an absence of reports of the use of MOF-supported nanoparticles for the production of functionalized anilines under mild conditions.

Herein, we report an efficient, convenient and high-yield protocol using MOF-supported palladium nanoparticles (Pd@MOF-1; Figure 1) as a catalyst for the reduction of nitroarenes under ambient conditions (Scheme 1).

## 2 | EXPERIMENTAL

### 2.1 | Synthesis of Pd@MOF-1

The synthesis procedure and crystal structure of MOF-1 are detailed in the supporting information according to the literature.<sup>[15]</sup> Pd@MOF-1 was prepared using a wet chemical method. To 50 mg of activated MOF-1 in 30 ml of ethanol, 4.2 mg ( $2.4 \times 10^{-2}$  mmol) of PdCl<sub>2</sub> in 10 ml of ethanol was added drop by drop. The mixture was kept stirring at room temperature for 2 hours to adsorb the Pd<sup>2+</sup> ions into MOF-1. Subsequently, 4.5 mg (12 mmol, 5 equiv. with respect to PdCl<sub>2</sub>) of NaBH<sub>4</sub> was added for the reduction of Pd<sup>2+</sup> ions with constant stirring for another 1 hour. Finally, the mixture was filtered and washed three times with fresh ethanol. The grey



**SCHMENE 1** Reduction of nitroarenes [Colour figure can be viewed at [wileyonlinelibrary.com](http://wileyonlinelibrary.com)]

solid was then dried under vacuum at 313 K. The amount of Pd adsorbed into MOF-1 was estimated with inductively coupled plasma atomic emission spectrometry (ICP-AES).

### 2.2 | General procedure for hydrogenations

In a typical protocol, the nitroarene compound (1 mmol) and the Pd@MOF-1 catalyst (1 mol%) were added into oven-dried glassware that was sealed with a rubber septum. Then, the reaction mixture was stirred under a hydrogen atmosphere with IKA RCT basic magnetic stirrer bars at 25°C after degasification (flushed with high-purity argon three times to remove O<sub>2</sub>). Completion of the reaction was monitored by TLC. After the completion of the reaction, the catalyst was removed from the solution by filtration, and the obtained filtrate was analyzed using LC-MS and purified by silica gel chromatography using an appropriate eluent for NMR analysis. Every experiment was conducted twice to ensure accuracy. The characterization data of <sup>1</sup>H NMR and <sup>13</sup>C NMR spectra of products are provided in the supporting information.

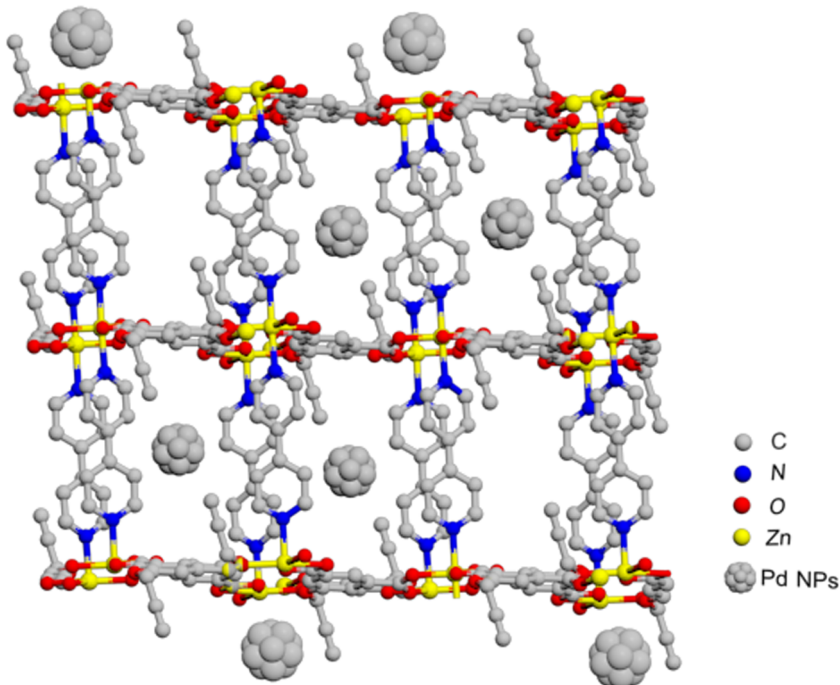


**FIGURE 1** Structure of Pd@MOF-1 [Colour figure can be viewed at [wileyonlinelibrary.com](http://wileyonlinelibrary.com)]

## 2.3 | Recycling of Pd@MOF-1 for hydrogenations

After the completion of the reaction, the catalyst was removed from the solution by filtration. The catalyst was washed three times with ethanol. The grey solid was dried under vacuum at 313 K for 3 hours to remove the residual solvent, and then reused as the catalyst in a subsequent run. The recyclability of the Pd@MOF-1 catalyst was investigated for the hydrogenation of nitrobenzene under the same reaction conditions mentioned before.

## 3 | RESULTS AND DISCUSSION

### 3.1 | Characterization of materials

A solvent infiltration method was adopted to load Pd nanoparticles into MOF-1 in a stepwise manner starting from  $\text{PdCl}_2$  precursor. To obtain further insight into the adsorption process, transmission electron microscopy (TEM), scanning electron microscopy (SEM) and the corresponding energy-dispersive X-ray spectroscopic (EDS) mapping were carried out using  $\text{Pd}^{2+}$ -adsorbed MOF-1 ( $\text{PdCl}_2@\text{MOF-1}$ ). SEM-EDS mapping analyses (Figure 2) of  $\text{PdCl}_2@\text{MOF-1}$  showed a uniform distribution of Zn, Pd and Cl throughout the entire MOF-1 crystal and demonstrated that the  $\text{Pd}^{2+}$  was uniformly dispersed with no accumulation in specific areas. Moreover, TEM analyses of  $\text{PdCl}_2@\text{MOF-1}$  showed no notably

congregated Pd particles, which indicated that the  $\text{Pd}^{2+}$  ions were adsorbed homogeneously (Figure 3). Such an even distribution may be because the ethynyl moieties responsible for stabilizing Pd nanoparticles were homogeneously present in every channel of MOF-1. A TEM image of Pd@MOF-1 is shown in Figure 4a. It shows that the distribution of Pd particles did not change after the reduction. The size of the Pd nanoparticles in the as-prepared Pd@MOF-1 catalyst is in the range 1–2 nm (Figure 4b).

X-ray photoelectron spectroscopy (XPS) is an excellent tool for confirming the change in the valence of metal ions. In this case, the Pd 3d spectra of  $\text{PdCl}_2@\text{MOF-1}$  and Pd@MOF-1 were obtained to confirm

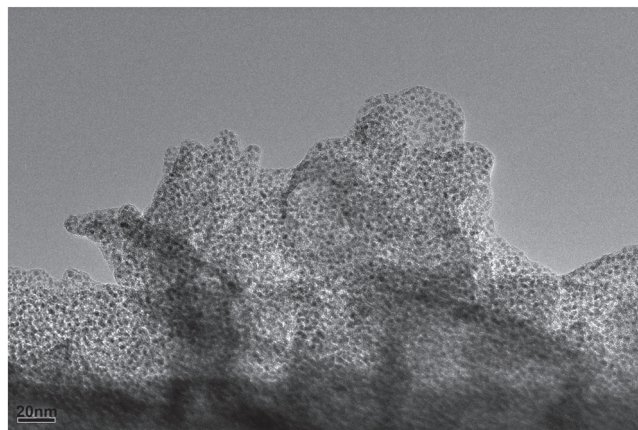


**FIGURE 3** TEM image of  $\text{PdCl}_2@\text{MOF-1}$

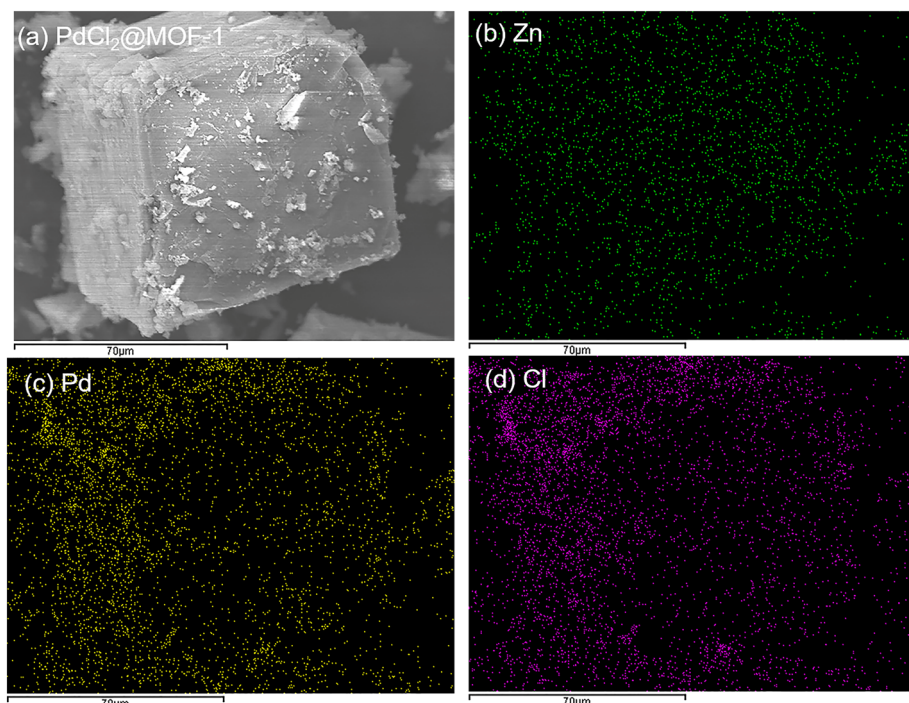


**FIGURE 2** SEM-EDS mapping of  $\text{PdCl}_2@\text{MOF-1}$  [Colour figure can be viewed at [wileyonlinelibrary.com](http://wileyonlinelibrary.com)]

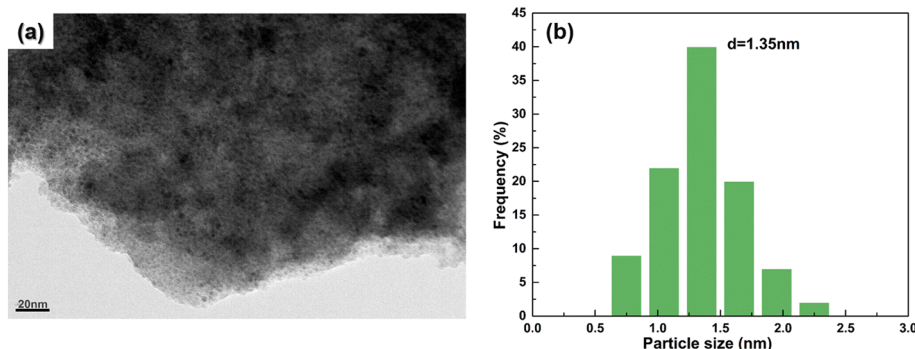


**FIGURE 4** (a) TEM image of Pd@MOF-1. (b) Particle size distribution of Pd@MOF-1 [Colour figure can be viewed at [wileyonlinelibrary.com](http://wileyonlinelibrary.com)]

the variation in valence in the Pd species and the role of NaBH<sub>4</sub>. As shown in Figure 5, two obvious peaks were observed in the Pd 3d spectrum of PdCl<sub>2</sub>@MOF-1, with binding energies of 338.3 and 343.6 eV that corresponded to the characteristics of Pd(II). This indicated that all Pd species in PdCl<sub>2</sub>@MOF-1 existed in the form of Pd<sup>2+</sup> before the reduction treatment of NaBH<sub>4</sub>. After reduction, the peaks of Pd 3d<sub>5/2</sub> and Pd 3d<sub>3/2</sub> appeared at binding energies of 335.3 and 340.7 eV, which demonstrated the formation of Pd nanoparticles.<sup>[15]</sup>

The formation of Pd nanoparticles was also confirmed from powder X-ray diffraction (PXRD) analysis (Figure 6). The high-angle broad peaks at 40.1° and 46.3° in the PXRD pattern of Pd@MOF-1 were ascribed to the face-centered cubic Pd (111) and (200) planes, indicating the formation of Pd nanoparticles. However, no characteristic diffraction peaks of face-centered cubic Pd nanoparticles at 67.6°, 81.2° and 85° were found, which indicated that Pd nanoparticles may be well dispersed. The PXRD pattern of Pd@MOF-1 also confirmed that the crystallinity of MOF-1 remained intact after Pd insertion.<sup>[15]</sup>

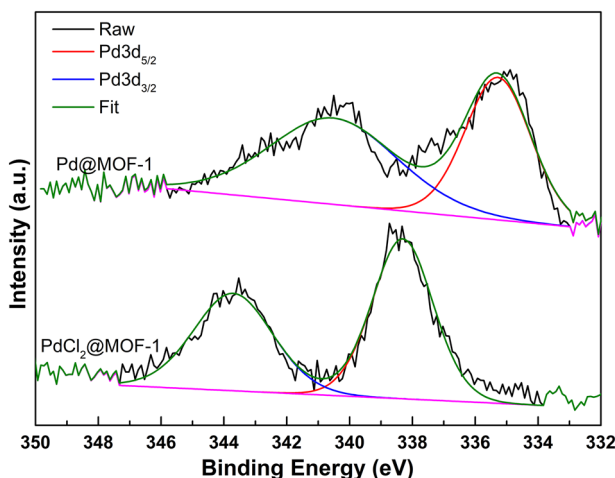


**FIGURE 5** Pd 3d core-level XPS spectra of PdCl<sub>2</sub>@MOF-1 and Pd@MOF-1 [Colour figure can be viewed at [wileyonlinelibrary.com](http://wileyonlinelibrary.com)]

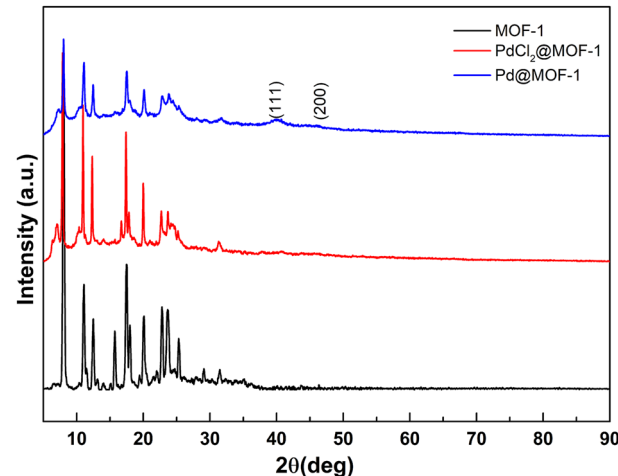


**FIGURE 6** Comparison of PXRD patterns of MOF-1, PdCl<sub>2</sub>@MOF-1 and Pd@MOF-1 [Colour figure can be viewed at [wileyonlinelibrary.com](http://wileyonlinelibrary.com)]

### 3.2 | Catalytic hydrogenation of nitroarenes

After the successful synthesis of the catalyst, we endeavored to identify the best catalytic system for the reduction of nitroarenes using nitrobenzene as a model substrate. As evident from Table 1, the solvent had a strong effect on the catalytic efficiency in this catalytic system; methanol and ethanol gave 88% and 98% yields within 2 hours, respectively (Table 1). Among the others, dimethylformamide and tetrahydrofuran gave reaction products in moderate yields (60% and 44%, respectively). The reaction occurred slowly in toluene. Considering the requirements of green development, ethanol was herein selected as the optimal solvent.

Based on the optimized reaction conditions, the catalytic activity of Pd@MOF-1 for the hydrogenation of nitrobenzene was evaluated. Pd@MOF-1 exhibited higher activity compared with commercial Pd/C catalyst (Table 2) and other reported Pd heterogeneous catalysts (supporting information, Table S2). To investigate the origin of the superior catalytic activity of Pd@MOF-1, the

**TABLE 1** Effect of various solvents for the reduction of nitrobenzene using Pd@MOF-1<sup>a</sup>

Entry	Solvent	Time (h)	Yield (%) <sup>b</sup>
1	Ethanol	2	98
2	Methanol	2	88
3	Dimethylformamide	2	60
4	Tetrahydrofuran	2	44
5	Toluene	2	15

<sup>a</sup>Reaction conditions: nitrobenzene (1 mmol), catalyst (1 mol%), solvent (8 ml), room temperature, H<sub>2</sub> balloon.

<sup>b</sup>Isolated yield.

**TABLE 2** Catalytic hydrogenation of nitrobenzene<sup>a</sup>

Entry	Catalyst	Time (h)	Yield (%) <sup>b</sup>
1	Pd@MOF-1	2	98
2	Pd/C	2	15
3	Pd nanoparticles	2	10
4	MOF-1	2	—

<sup>a</sup>Reaction conditions: nitrobenzene (1 mmol), catalyst (1 mol%), ethanol (8 ml), room temperature, H<sub>2</sub> balloon.

<sup>b</sup>Isolated yield.

specific surface areas of Pd@MOF-1 and Pd/C were measured via nitrogen adsorption. As depicted in Figure S3, the surface area of the Pd/C catalyst was estimated to be 871.9 m<sup>2</sup> g<sup>-1</sup>, that of the Pd@MOF-1 catalyst being only 23.9 m<sup>2</sup> g<sup>-1</sup>. In consideration of good porosity observed from the single-crystal X-ray structure,<sup>[15]</sup> a fraction of the pores accessible to H<sub>2</sub> molecules may not be accessible to N<sub>2</sub> molecules especially at cryogenic temperatures,<sup>[19]</sup> hydrogen sorption measurements being conducted at 298 K. The H<sub>2</sub> adsorption ability of Pd@MOF-1 is much better than that of Pd/C as expected (Figure S4), revealing that MOF-1 plays very important roles in H<sub>2</sub> adsorption. To examine this assumption, free-standing Pd nanoparticles were prepared using the same method as for Pd@MOF-1. As shown in Figure S4, the H<sub>2</sub> adsorption ability of Pd@MOF-1 is dozens of times that of the Pd nanoparticles.

Control reactions over MOF-1 or Pd nanoparticles were also carried out. The results show that the activity of MOF-1 is negligible (Table 2). The use of Pd@MOF-1 leads to almost complete conversion of nitrobenzene in 120 minutes, whereas only 10% conversion occurred in the presence of Pd nanoparticles under otherwise identical reaction conditions. The significant difference could be partially due to the H<sub>2</sub> enrichment capability of MOF-1 (Figure S4). Meanwhile, the TEM images of the Pd nanoparticles (Figure S5) show that the Pd nanoparticles are mostly agglomerated without the stabilization of the

support. The mean size of Pd nanoparticles is 12.72 nm, revealing that MOF-1 is crucial for stabilizing the metal nanoparticles.

In addition, the results presented in Table 2 show that the size of Pd (Figure 4 and Figure S5) in those samples increased in an order opposite to that of the catalytic activity (Pd@MOF-1 > Pd/C > Pd nanoparticles). This could be rationalized by the fact that smaller particles possess a larger number of surface atoms that can improve the conversion rate of the catalytic reaction. Considering all of these results, the superior catalytic activity of Pd@MOF-1 was attributed to the MOF-1 as support. MOF-1 can not only act as a stabilizer for metal nanoparticles, but also enable the superior H<sub>2</sub> enrichment property of the catalyst which would effectively enhance the catalytic efficiency, as also demonstrated in previous reports.<sup>[20]</sup>

To establish the scope of the catalyst, several nitroarenes were adopted under the same reaction conditions, with the results summarized in Table 3. It was obvious that the compounds were reduced with high yields regardless of the diversity of structure (Table 3, entries 2–19). Alkyl-substituted nitroarenes showed high conversion, with up to 96% yield (Table 3, entries 2–4). However, the activity was significantly influenced by the position of the substituents on the aromatic ring. For example, the decreased reaction rate of *ortho*-methylnitrobenzene relative to the *meta* and *para* analogues demonstrates a steric effect (Table 3, entries 2–4). Moreover, naphthalene-substituted nitroarenes took more time (5 hours) than methyl-substituted nitroarenes (2–3 hours) but were still capable of producing good yields (89%; Table 3, entry 5).

In general, electron withdrawing/donating groups, such as nitro and methoxy groups, did not have a significant influence on the reaction. For instance, 4-nitroanisole, 4-nitrothioanisole, 3,4-dimethoxynitrobenzene and 4-methoxy-3-methylnitrobenzene were equally well transformed into the corresponding anilines (Table 3, entries 6–9). Notably, the presence of sulfur atoms resulted in a slower reaction rate; it took three times longer (6 hours) than nitrobenzene to reduce thioether (Table 3, entry 7). Moreover, diaminobenzene was easily accessible from the corresponding dinitrobenzene (Table 3, entries 10 and 11).

The catalyst also showed promise for selective reduction of substrates bearing other reducible groups (Table 3, entries 10–17). Esters and ketones remained untouched under the reaction conditions (Table 3, entries 13–15). The activities of 3-nitroacetophenone and 4-nitroacetophenone were slightly influenced by the nature/position of the substituents on the aromatic ring (Table 3, entries 14 and 15). In addition, nitroarenes bearing

**TABLE 3** Reduction of various nitroarenes using Pd@MOF-1<sup>a</sup>

Entry	Substrate	Time (h)	Yield (%) <sup>b</sup>	Entry	Substrate	Time (h)	Yield (%) <sup>b</sup>
1	Nitrobenzene	2	98	13	Methyl 4-nitrobenzoate	3	96
2	4-Nitrotoluene	2	96	14	4-Nitroacetophenone	3	96
3	3-Nitrotoluene	2	96	15	3-Nitroacetophenone	3	90
4	2-Nitrotoluene	3	94	16	4-Nitrobenzamide	3	91
5	1-Nitronaphthalene	5	89	17	4-Nitrobenzaldehyde	5	82
6	4-Nitroanisole	3	92	18 <sup>d</sup>	4-Nitrochlorobenzene	6	76
7	4-Nitrothioanisole	6	96	19 <sup>e</sup>	4-Iodonitrobenzene	6	84
8	3,4-Dimethoxynitrobenzene	4	90	20	5-Nitroquinoline	4	87
9	4-Methoxy-3-methylnitrobenzene	4	90	21	5-Nitroisoquinoline	3	90
10 <sup>c</sup>	1,4-Dinitrobenzene	6	89	22	6-Nitroquinoline	4	90
11 <sup>c</sup>	1,3-Dinitrobenzene	6	86	23	7-Nitroquinoline	3	96
12	2-(4-Nitrophenyl)ethanol	5	91	24 <sup>[c]</sup>	8-Nitroquinoline	3	—

<sup>a</sup>Reaction conditions: substrate (1 mmol), catalyst (1 mol%), ethanol (8 ml), room temperature, H<sub>2</sub> balloon.

<sup>b</sup>Isolated yield.

<sup>c</sup>50°C.

<sup>d</sup>20% of aniline product was obtained.

<sup>e</sup>13% of aniline product was obtained.

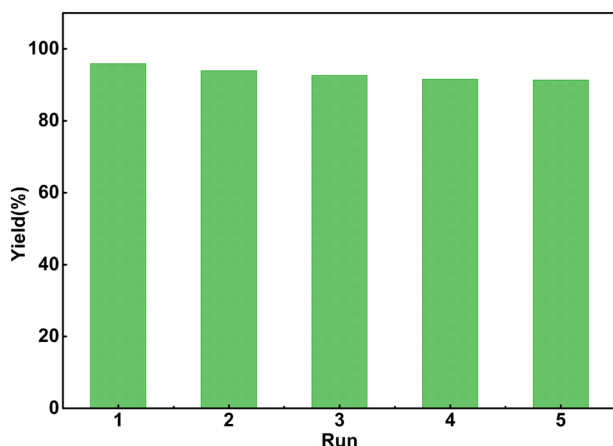


**FIGURE 7** Recycling of Pd@MOF-1 for reduction of nitrobenzene [Colour figure can be viewed at [wileyonlinelibrary.com](http://wileyonlinelibrary.com)]

amides showed excellent conversion, producing the corresponding anilines (Table 3, entry 16). 4-Nitrobenzaldehyde bearing a sensitive aldehyde functionality

was smoothly reduced with high selectivity affording the corresponding aniline in 82% yield (Table 3, entry 17). For halide-containing substrates, little hydrogenolysis of the C&bond;X bond was observed (Table 3, entries 18 and 19), but still retaining good yields (>76%).

Heterocyclic compounds, such as quinolines, were successfully employed. Mononitro-substituted quinolines were chemoselectively hydrogenated in good to excellent yields (87–96%), regardless of the position of the nitro substituent on the benzene ring (Table 3, entries 20–23). Interestingly, compared with other quinolines mentioned before (Table 3, entries 20–23), the substrate bearing a nitro group at the 8-position exhibited extremely low reactivity, TLC showing no new spot after 3 hours with slight heating.

Stability is an essential characteristic of an excellent catalyst in a solid–liquid reaction, particularly when the reactant or the product has a strong interaction with the supported metal particles, which may accelerate the leaching of metal nanoparticles from the supports.<sup>[21]</sup>

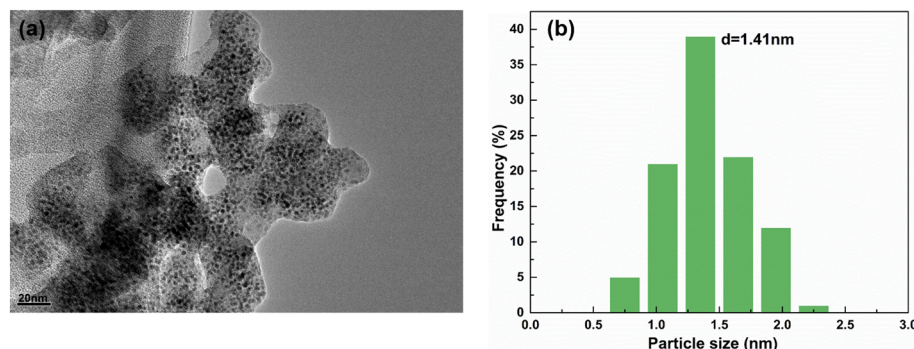


**FIGURE 8** (a) TEM image of recovered Pd@MOF-1 after the fifth catalytic cycle. (b) Particle size distribution of recovered Pd@MOF-1 [Colour figure can be viewed at [wileyonlinelibrary.com](http://wileyonlinelibrary.com)]

The stability of Pd@MOF-1 was further investigated using recycling experiments, and the results are depicted in Figure 7. Pd@MOF-1 demonstrated stable recovery by simple filtration from the reaction mixture. Only a negligible decline (1–3%) in the catalytic activity of Pd@MOF-1 was observed when the catalyst was used for five successive cycles in the hydrogenation of nitrobenzene.

Moreover, the average particle diameter and size distribution of freshly prepared Pd@MOF-1 catalyst and of catalyst after the fifth cycle were compared. TEM analyses of the Pd@MOF-1 catalyst after reuse showed particle size and size distribution (mean size = 1.41 nm) similar to those of the freshly prepared catalyst, and no agglomeration of the used catalyst was observed (Figure 8). XPS analysis revealed no shift in the binding energy of Pd nanoparticles (Table S3). These observations confirmed that the catalyst was suitably active for up to five cycles.

To confirm the heterogeneous nature of the Pd@MOF-1 catalyst, Pd@MOF-1 was removed from the reaction mixture by simple filtration at a 15% conversion of nitrobenzene. The filtrate was used for reaction under similar conditions; however, it showed no further conversion of nitrobenzene. No leaching of Pd atoms in the filtrate was verified using ICP-AES analysis (detection limit of 0.10 ppm).

## 4 | CONCLUSIONS

In summary, the general reduction of nitroarenes to the corresponding amines in good to excellent yields (76–98%) was achieved using Pd nanoparticles supported on MOF. This method was easy and exceedingly efficient. A large range of reducible functional groups was tolerated under these reaction conditions. Other notable advantages of this catalytic system included high isolated yields, the use of hydrogen as a sustainable source, an easy handling procedure and the reusability of the catalyst.

## ACKNOWLEDGMENTS

The authors acknowledge financial support from the National Natural Science Foundation of China (21576026 and 21975023).

## CONFLICT OF INTEREST

There are no conflicts to declare.

## ORCID

Lingxiang Bao  <https://orcid.org/0000-0001-5473-6791>

## REFERENCES

- [1] (a)S. F. Cai, H. H. Duan, H. P. Rong, D. S. Wang, L. S. Li, W. He, Y. D. Li, *ACS Catal.* **2013**, *3*, 608. (b)Z. Z. Wei, J. Wang, S. J. Mao, D. F. Su, H. Y. Jin, Y. H. Wang, F. Xu, H. R. Li, Y. Wang, *ACS Catal.* **2015**, *5*, 4783. (c)M. Orlandi, D. Brenna, R. Harms, S. Jost, M. Benaglia, *Org. Process Res. Dev.* **2016**, *22*, 430. (d)J. H. Kim, J. H. Park, Y. K. Chung, K. H. Park, *Adv. Synth. Catal.* **2012**, *354*, 2412. (e)Z. C. Ding, C. Y. Li, J. J. Chen, J. H. Zeng, H. T. Tang, Y. J. Ding, Z. P. Zhan, *Adv. Synth. Catal.* **2017**, *359*, 2280.
- [2] (a)R. J. Rahaim, R. E. Maleczka, *Org. Lett.* **2005**, *7*, 5087. (b)A. Corma, P. Serna, P. Concepcion, J. J. Calvino, *J. Am. Chem. Soc.* **2008**, *130*, 8748.
- [3] (a)L. Q. Liu, B. T. Qiao, Z. J. Chen, J. Zhang, Y. Q. Deng, *Chem. Commun.* **2009**, 653. (b)H. S. Wei, X. Y. Liu, A. Q. Wang, L. L. Zhang, B. T. Qiao, X. F. Yang, Y. Q. Huang, S. Miao, J. Y. Liu, T. Zhang, *Nat. Commun.* **2014**, *5*, 5634.
- [4] (a)S. Chandrappa, K. Vinaya, T. Ramakrishnappa, K. S. Rangappa, *Synlett* **2010**, *20*, 3019. (b)K. M. Doxsee, M. Feigel, K. D. Stewart, J. W. Canary, C. B. Knobler, D. J. Cram, *J. Am. Chem. Soc.* **1987**, *109*, 3098. (c)F. A. Khan, J. Dash, C. Sudheer, R. K. Gupta, *Tetrahedron Lett.* **2003**, *44*, 7783.
- [5] A. Corma, C. Gonza'lez-Arellano, M. Iglesias, F. I. Sa'nchez, *Appl. Catal. A* **2009**, *356*, 99.
- [6] O. Mazaheri, R. J. Kalbasi, *RSC Adv.* **2015**, *5*, 34398.
- [7] (a)R. V. Jagadeesh, G. Wienhofer, F. A. Westerhaus, A. E. Surkus, M. M. Pohl, H. Junge, K. Junge, M. Beller, *Chem. Commun.* **2011**, *47*, 10972. (b)P. Ryabchuk, K. Junge, M. Beller, *Synthesis* **2018**, *50*, 4369. (c)Y. N. Duan, X. S. Dong, T. Song, Z. Z. Wang, J. L. Xiao, Y. Z. Yuan, Y. Yang, *ChemSusChem* **2019**, *12*, 4636.
- [8] P. N. Sathishkumar, N. Raveendran, N. S. P. Bhuvanesh, R. Karvembu, *J. Organometal. Chem.* **2018**, *876*, 57.
- [9] (a)F. A. Westerhaus, I. Sorribes, G. Wienhöfer, K. Junge, M. Beller, *Synlett* **2015**, *26*, 313. (b)Y. N. Duan, T. Song, X. S. Dong, Y. Yang, *Green Chem.* **2018**, *20*, 2821. (c)T. Song, P. Ren, Y. N. Duan, Z. Z. Wang, X. F. Chen, Y. Yang, *Green Chem.* **2018**, *20*, 4629.
- [10] J. T. Wang, X. C. Yu, C. Y. Shi, D. J. Lin, J. Li, H. L. Jin, X. Chen, S. Wang, *Adv. Synth. Catal.* **2019**, *361*, 1.
- [11] J. R. Morse, J. F. Callejas, A. J. Darling, R. E. Schaak, *Chem. Commun.* **2017**, *53*, 4807.
- [12] (a)B. Tang, W. C. Song, E. C. Yang, X. J. Zhao, *RSC Adv.* **2016**, *7*, 1531. (b)K. Shen, L. Chen, J. L. Long, W. Zhong, Y. W. Li, *ACS Catal.* **2015**, *5*, 5264. (c)P. Hester, S. J. Xu, W. Liang, N. Al-Janabi, R. Vakili, P. Hill, C. A. Muryn, X. B. Chen, P. A. Martin, X. L. Fan, *J. Catal.* **2016**, *340*, 85. (d)Y. Y. Pan, B. Z. Yuan, Y. W. Li, D. H. He, *Chem. Commun.* **2010**, *46*, 2280.
- [13] H. L. Liu, L. N. Chang, C. H. Bai, L. Y. Chen, L. Q. R, Y. W. Li, *Angew. Chem.* **2016**, *55*, 5019.
- [14] X. D. Chen, K. Shen, D. N. Ding, J. Y. Chen, T. Fan, R. F. Wu, Y. W. Li, *ACS Catal.* **2018**, *8*, 10641.
- [15] (a)B. Gole, U. Sanyal, P. S. Mukherjee, *Chem. Commun.* **2015**, *51*, 4872. (b)B. Gole, U. Sanyal, R. Banerjee, P. S. Mukherjee, *Inorg. Chem.* **2016**, *55*, 2345.
- [16] (a)Y. Luan, Y. Qi, H. Gao, N. N. Zheng, G. Wang, *J. Mater. Chem. A* **2014**, *2*, 20588. (b)J. Zhu, P. C. Wang, M. Lu, *Appl.*

- Catal. A* **2014**, *477*, 125. (c)X. Qiu, W. Zhong, C. H. Bai, Y. W. Li, *J. Am. Chem. Soc.* **2016**, *138*, 1138.
- [17] L. J. Shen, W. M. Wu, R. W. Liang, R. Lin, L. Wu, *Nanoscale* **2013**, *5*, 9374.
- [18] (a)J. L. Long, B. L. Yin, Y. W. Li, L. J. Zhang, *AICHE* **2014**, *60*, 3565. (b) L. Luz, C. Rösle, K. Epp, F. X. L. i. Xamena, R. A. Fischer, *Eur. J. Inorg. Chem.* **2015**, *2015*, 3904.
- [19] J. Jagiello, C. O. Ania, J. B. Parra, L. Jagiello, J. J. Pis, *Carbon* **2007**, *45*, 1066.
- [20] (a)X. B. Xu, Z. C. Zhang, X. Wang, *Adv. Mater.* **2015**, *27*, 5365. (b)Q. H. Yang, Q. Xu, S. H. Yu, H. L. Jiang, *Angew. Chem. Int. Ed.* **2016**, 3685. (c)Y. G. Huang, Q. H. Yang, Q. Xu, S. H. Yu, H. L. Jiang, *Angew. Chem. Int. Ed.* **2016**, 7379.
- [21] Z. L. Li, J. L. Li, J. H. Liu, Z. L. Zhao, C. G. Xia, F. W. Li, *ChemCatChem* **2014**, *6*, 1333.

## SUPPORTING INFORMATION

Additional supporting information may be found online in the Supporting Information section at the end of this article.

**How to cite this article:** Bao L, Yu Z, Fei T, et al. Palladium supported on metal–organic framework as a catalyst for the hydrogenation of nitroarenes under mild conditions. *Appl Organometal Chem.* 2020;e5607. <https://doi.org/10.1002/aoc.5607>